RESEARCH PAPER

Biomatter 5:1, e1056943; August 2015; Published with license by Taylor and Francis Group, LLC

Small-sized granules of biphasic bone substitutes support fast implant bed vascularization

M Barbeck[1,2,*], M Dard[3], M Kokkinopoulou[4], J Markl[4], P Booms[1], RA Sader[1], CJ Kirkpatrick[1,2], and S Ghanaati[1,2]

[1]Institute of Pathology; Repair-Lab; University Medical Center of the Johannes Gutenberg University; Mainz, Germany; [2]Department for Oral; Cranio-Maxillofacial and Facial Plastic Surgery; FORM-Lab, Medical Center of the Goethe University; Frankfurt am Main, Germany; [3]Department of Periodontology and Implant Dentistry; New York University; New York, NY USA; [4]Institute for Zoology; Johannes Gutenberg-University; Mainz, Germany

Keywords: biphasic bone substitute, BoneCeramic, degradation, granule size, multinucleated giant cells, phagocytosis, vascularization

The present study investigated the influence of granule size of 2 biphasic bone substitutes (BoneCeramic® 400–700 μm and 500–1000 μm) on the induction of multinucleated giant cells (MNGCs) and implant bed vascularization in a subcutaneous implantation model in rats. Furthermore, degradation mechanisms and particle phagocytosis of both materials were examined by transmission electron microscopy (TEM). Both granule types induced tissue reactions involving primarily mononuclear cells and only small numbers of MNGCs. Higher numbers of MNGCs were detected in the group with small granules starting on day 30, while higher vascularization was observed only at day 10 in this group. TEM analysis revealed that both mono- and multinucleated cells were involved in the phagocytosis of the materials. Additionally, the results allowed recognition of the MNGCs as the foreign body giant cell phenotype. Histomorphometrical analysis of the size of phagocytosed particles showed no differences between the 2 granule types. The results indicate that granule size seems to have impact on early implant bed vascularization and also on the induction of MNGCs in the late phase of the tissue reaction. Furthermore, the results revealed that a synthetic bone substitute material can induce tissue reactions similar to those of some xenogeneic materials, thus pointing to a need to elucidate their "ideal" physical characteristics. The results also show that granule size in the range studied did not alter phagocytosis by mononuclear cells. Finally, the investigation substantiates the differentiation of material-induced MNGCs, which are of the foreign body giant cell type.

Introduction

In recent decades, synthetic bone substitute materials have been extensively shown to be good alternatives to autologous bone grafts, which are still considered to be the regenerative "gold standard".[1,2] Calcium phosphates, specifically hydroxyapatite (HA) and β-tricalcium phosphate (β-TCP), are primarily used because of their chemical similarity to the calcified bone matrix and the related osteoconductive regeneration mechanisms.[3,4] However, it has been shown that these 2 ceramics exhibit different resorption patterns characterized by different dissolution properties and degrees of induction of phagocytosis based on mono- and multinucleated cells.[5,6] Furthermore, it has been demonstrated that bone substitute materials based on HA can persist for many years within their implantation beds, while those based on β-TCP are subjected to rapid degradation.[5,7] Both resorption patterns do not result in an optimal standing time in keeping with the theory of guided bone regeneration (GBR) that calls for a balanced resorption pattern parallel to the ingrowth of bone tissue.[5,7] Within synthetic bone substitute materials, so-called biphasic materials that are mixtures of HA and β-TCP have been shown to exhibit an intermediate level of biodegradation.[5-7] A previous study by our group revealed that a biphasic bone substitute material with a HA/β-TCP ratio of 60/40 combined the inflammatory and degradation characteristics of the 2 compounds.[6] It was observed that high numbers of multinucleated giant cells and high vascularization rates were induced within the first 15 d after implantation, comparable to the results of pure β-TCP. However, after 15 d, the extent of multinucleated giant cell formation and vascularization changed and were comparable to properties of HA material until the end of the study. Based on these results, it was concluded that bone substitute material with mixtures of both calcium phosphate compounds are favorable candidates for clinical application.

In addition to the chemical composition, an "optimal" bone substitute material must also possess a specific combination of physical properties to support an optimal bone regeneration process by promoting the ingrowth of osteoblasts, endothelial cells

*Correspondence to: M Barbeck; Email: mike.barbeck@kgu.de
Submitted: 03/02/2015; Revised: 05/11/2015; Accepted: 05/26/2015
http://dx.doi.org/10.1080/21592535.2015.1056943

and other cells involved in bone growth, as well as cells involved in material degradation.[8] Material factors such as the porosity, surface structure and shape of the material granules have been identified as determining factors in material-mediated bone growth and degradation.[8-14] Among these properties the granule size of the bone substitute material is also assumed to exert a large influence on its regenerative potential, as it is expected to govern the material resorbability.[8] A variety of *in vitro* and *in vivo* studies have been conducted to quantify the impact of this factor on the progress and outcome of bone regeneration, but no definitive conclusions have thus far been reached.[14-30]

Following previous studies conducted by our group analyzing tissue reactions to bone substitute materials with a special focus on their chemical composition and physical characteristics, the present study investigates the influence of granule size of a biphasic bone substitute material. In this investigation 2 granule sizes of BoneCeramic® (500–1000 μm and 400–700 μm) were tested with respect to the tissue reaction in a subcutaneous implantation model in Wistar rats over a 60 day period. Additionally, the cellular biodegradation mechanism of the bone substitute materials was investigated by means of transmission electron microscopy (TEM).

Materials and Methods

Bone grafting substitutes

The physicochemical specifications of the 2 synthetic bone substitute material are given as a mixture of 60% hydroxyapatite (HA) and 40% β-tricalcium phosphate (β-TCP).[31] Both granule types were manufactured from the same precursor material, which was crushed and separated by sieving to control the granule diameter ranges, with one material stated to have granule diameters between 500–1000 μm (BoneCeramic® 500–1000 μm), and the other between 400–700 μm (BoneCeramic® 400–700 μm).[30] All other material characteristics such as the chemical composition, shape, morphology and porosity of the granules are supposed to be identical for the 2 products based on the common production process of both materials.[31]

Scanning electron microscopy *(SEM)*

To investigate the physical characteristics of the 2 granule types, scanning electron microscopy (SEM) was performed with a Zeiss Supra 55 scanning electron microscope (QS Nr. 57113, Carl Zeiss SMT AG, Oberkochen, Germany) with a field electron emitter.

X-ray diffraction (XRD) analysis

To determine the chemical composition X-ray diffraction (XRD) analysis was conducted using an X-ray diffractometer (PANalytic X'Pert MPD, PANalytical, Almelo, Netherlands) with a fixed incident beam angle of 5° and a detector angle range of $5° < 2\theta < 80°$ in combination with the X'Pert High Score software. A Cu Kα (1.54184 A°) radiation at a voltage of 50 kV, a current of 40 mA, a step size of 0.02° and a scan rate of 1.2°/min were used.

In vivo experiments

Experimental design and subcutaneous implantation

The study was performed on 61 female 6–8 weeks old Wistar rats and 12 female 5-week-old SCID mice that were obtained from Military Medical Academy (Belgrade, Serbia) and with the approval of the Local Ethical Committee (Faculty of Medicine, University of Niš, Serbia). The animals were maintained for 1 week before use at the Faculty of Medicine, University of Niš, Serbia. Animals were kept under standard conditions with regular mouse pellets, access to water *ad libitum* and an artificial light–dark cycle of 12 h each.

The study protocol involved the random apportion of the Wistar rats into 3 experimental groups. 40 animals were used for the implantation of BoneCeramic® 500–1000 μm (BC 500–1000) and BoneCeramic® 400–700 μm (BC 400–700). 20 animals were assigned to each study group, and $n = 4$ animals per time point were allocated for subcutaneous implantation for each of the 5 study time points (3, 10, 15, 30 and 60 days). A third group of 15 animals with $n = 3$ animals per time point was used as control by operation without biomaterial to determine the inflammatory and wound-healing responses related to the operation procedure. Six additional rats ($n = 3$ per bone substitute material) were used for material implantation for further evaluation of the *in vivo* degradation behavior of the bone substitutes by transmission electron microscopy (TEM) 15 d after implantation.

Material implantation was conducted according to a previously established protocol.[6,14, 32-37] In brief, after initial intraperitoneal anesthesia (10 ml ketamine [50 mg(ml] with 1.6 ml xylazine [2%]), 60 mg of the selected bone substitute material was implanted under sterile conditions in a preformed subcutaneous pocket in the animal's subscapular region using a bone curette. Subsequently, the implantation wound was stitched with 5.0 Prolene (Ethicon, New Jersey, USA). The experimental animals were housed individually under the above-mentioned conditions until the explanation of the materials at the described time points.

Tissue preparation of the subcutaneous implantation pocket

After euthanasia of the animals by an overdose of a mixture of ketamine and xylazine, tissue preparation was conducted according to a previously described method.[6,14,32-37] Briefly, the implanted bone substitutes were explanted, fixed in 4% formalin for 24 hours and cut into 3 equal segments. After decalcification in 10% tris-buffered EDTA (Carl Roth, Karlsruhe, Germany) at 37°C for 5–10 d, subsequent dehydration in a series of increasing alcohol concentrations and xylol was carried out, and after paraffin embedding, the preparation of histological sections with a thickness of 3–5 μm was performed with a rotation microtome (Leica, Wetzlar, Germany).

Histochemical staining methods of animal tissue

Histochemical staining was also performed as previously described.[6,14,32-37] A first slide of each of the 3 tissue blocks from each animal was stained with hematoxylin and eosin (H&E) for general (histological) evaluation of the material implantation

beds. Based on these slides, the tissue block with the best cross-section of the implanted biomaterials and peri-implant tissue was selected for further slide preparation and staining, as well as histological and histomorphometrical analysis. A second section from this block was used to stain for tartrate-resistant acid phosphatase (TRAP) to identify so-called "osteoclast-like cells," multinucleated giant cells with TRAP expression. The third and fourth sections were stained using special connective tissue staining methods, i.e., Movat's Pentachrome and Azan, to enable a differentiated overview of the different tissue components within the implant beds of the bone substitute material as previously shown.[6,14, 32-37]

Immunohistochemistry

Two further sections of the above-mentioned tissue blocks were used for immunohistochemical detection of murine vessels within the implantation beds of the bone substitutes following established protocols.[6,14, 32-37] In brief, epitope retrieval was performed after blocking endogenous peroxidase using a 3% H_2O_2 – distilled water solution. CD31-staining was performed by using a monoclonal mouse anti-rat CD31 antibody (clone: TLD-3A12, Serotec, Puchheim, Germany) in combination with Dual Endogenous Enzyme Block Dako S2003 (Dako, Glostrup, Denmark). Finally, antigen sites were detected using diaminobenzidine as chromogen, and slides were counterstained with Mayer's hematoxylin for light microscopy. One of these slides was used as negative control and underwent incubation without the primary antibody.

Tissue preparation for TEM analysis

For transmission electron microscopy, a previously described method was carried out at the Institute for Zoology of the Johannes Gutenberg University Mainz.[38] In brief, the specific tissue regions within the bone substitute granules were cut into small pieces (3–6 mm^3). Subsequently, the tissue specimens were fixed in a freshly prepared medium of 1% glutaraldehyde in 0.1M cacodylate buffer pH 7.2 for a minimum of 2 h at room temperature. After rinsing in 0.1M cacodylate buffer, the material was post-fixed for 1 hour in 2% osmium tetroxide in 0.1M cacodylate buffer. Following washing in 0.1M cacodylate buffer and dehydration in ascending concentrations of ethanol, the samples were treated with propylene oxide and embedded in araldite. Ultrathin sections (70–100 nm) were cut on an ultramicrotome (Reichert Ultracut E, Leica Microsystems) and stained with 2% uranyl acetate for 10 min and lead citrate for 2 min.[39] Transmission electron micrographs were taken using a CCD camera (TVIPS) connected to a Tecnai12 transmission electron microscope at 120kV.

Qualitative histological analysis

Qualitative histopathological evaluation of the biomaterial-tissue interactions was conducted using a light microscope (Eclipse 80i, Nikon, Tokyo, Japan). The outcome of the tissue-biomaterial interaction in the specimens was evaluated by examination of the total implantation bed and its peri-implant tissue. Thereby, the extent of the early (3–15 days) and late inflammatory responses (30 and 60 days) induced by the biomaterials was described following an established research protocol to access the following characteristics[6,14, 32-37]: fibrosis, hemorrhage, necrosis, vascularization, presence of granulocytes, lymphocytes, plasma cells, monocytes/macrophages, and TRAP-negative and TRAP-positive multinucleated giant cells (MNGCs). Microphotographs were taken using a DS-Fi1 digital camera and a digital sight control unit (Nikon, Tokyo, Japan).

Histomorphometry (Quantitative histological analysis)

Histomorphometrical analysis, i.e., measurements of the implant bed vascularization and of the numbers of multinucleated giant cells (MNGCs), was performed following a standardized protocol.[6,14, 32-37] In brief, images of the total implantation beds ("total scans"), i.e., the implanted bone substitute granules in combination with their corresponding peri-implant tissue, were digitalized by means of a combination of an Eclipse 80i histological microscope (Nikon, Tokyo, Japan), a DS-Fi1 digital camera (Nikon, Tokyo, Japan) and an automatic scanning table (Prior, USA) connected to a computer. The resulting images ("total scans") had a 100× magnification and a resolution of 2500 × 1200 pixels. A CD31-stained slide as well as a TRAP slide from each experimental animal were digitalized for further quantitative analysis of vascularization and giant cell phenotypes.

The extent of vascularization within the implantation beds was studied using the *NIS-Elements* "*Annotations and Measurements*" tool by separately marking the blood vessels using the "*area*" tool. The software enables measurement of the area (in μm^2) as well as the mean diameter of the vessels (in μm). Subsequently, vessel density was calculated from the total number of vessels related to the total area of the specific implantation bed (vessels/mm^2). The percent vessel area was calculated by relating the area sum of all vessels to the total implantation area. For each time point, a mean number of vessels/mm^2 and a mean of the total vessel area were determined. The corresponding TRAP slides were also digitalized and used to count the number of material-adherent multinucleated giant cells and their subforms, i.e., TRAP-negative and TRAP-positive multinucleated giant cells. These cells were counted manually using the counting tool of the NIS Elements software, and the number of each cell fraction was then calculated by relating to the total implantation area of the respective slide (cell number/mm^2).

Histomorphometrical measurement of particle phagocytosis

The figures obtained via transmission electron microscopy in the second part of the study enabled the measurement of material particle sizes phagocytosed by the mononuclear cells. In brief, measurements of the particle size were taken using the area tool of the NIS-Elements "*Annotations and Measurements*" section. Unfortunately, measurement of the particles phagocytosed by the multinucleated giant cells was limited due to the hardness of the bone substitutes and associated issues with sectioning of the araldite-embedded explants. Thus, large cells, such as multinucleated giant cells, tended to fragment on sectioning.

Statistical Analysis

Quantitative histomorphometrical data were statistically tested by an analysis of variance (ANOVA) followed by an LSD post-hoc assessment to compare groups using SPSS 16.0.1 software (SPSS Inc., Chicago, IL). Inter- (*) and intraindividual (•) differences were considered significant if P-values were less than 0.05 (*/• $P<0.05$), and highly significant if P-values less than 0.01 (**/•• $P<0.01$) or less than 0.001 (***/••• $P<0.001$). The data were presented as the mean ± standard deviation using GraphPad Prism 6.0c software (GraphPad Software Inc., La Jolla, USA).

Results

Physicochemical analyses

Physical characteristics of the bone substitutes

The results of the physical examination by means of scanning electron microscopy (SEM) confirmed that the granules of the 2 analyzed bone substitute materials differed in their size (**Fig. 1** A1 and B1). However, no differences were observed in shape (**Fig. 1** A1, 1 B1 and 1 A2, 1 B2), surface structure, or pore distribution of these bone substitute granules (**Fig. 1** A3, 1 B3 and 1 A4, 1 B4).

The SEM examinations additionally showed that the granules of the synthetic materials featured a characteristic morphology reminiscent of the trabecular bone matrix (**Fig. 1** A1, 1 B1 and 1 A2, 1 B2). Both granule types had an approximately octagonal shape with depressions within their walls (**Fig. 1** A1, 1 B1 and 1 A2, 1 B2). However, only cup-like fragments of these octagonal balls were observed, probably as a result of the fragmentation process (**Fig. 1** A1 and B1). Regularly larger pores were observable in the depressions in the sidewalls (**Fig. 1** A1 and B1). The surface structure was relatively smooth, and only sporadic micropores with diameters of merely a few micrometers were found (**Fig. A3 and B3**).

Chemical characteristics of the bone substitute granules

The analysis of the chemical composition of the bone substitute granules by means of X-ray diffraction revealed a phase composition of 61.6% hydroxyapatite (HA) and 38.4% β-tricalcium phosphate (β-TCP) for both granule sizes (data not presented). Hence, no differences between the mix ratios of the 2 bone substitutes were found.

***In vivo* study**

All experimental animals survived the surgical procedures without any postoperative complications. No signs of necrosis or severe inflammatory responses were observed at any of the study time points.

Qualitative histological results

Tissue reaction of the sham-operated animals. On day 3 after implantation, the tissue around the control incisions contained large numbers of mononuclear cells (macrophages, lymphocytes, granulocytes and fibroblasts) as well as numerous vessels (data not presented). The number of cells within this area was visibly larger than in unaffected areas of the subcutaneous connective tissue. Between day 10 and day 30 after implantation, the number of the above-described cells decreased within the tissue surrounding incision. By day 60 after implantation, no histological signs of the tissue defects induced by the control incisions were visible, and a regular distribution of resident cells and extracellular matrix was attained. No multinucleated giant cells were observed at any of the time points studied (data not presented).

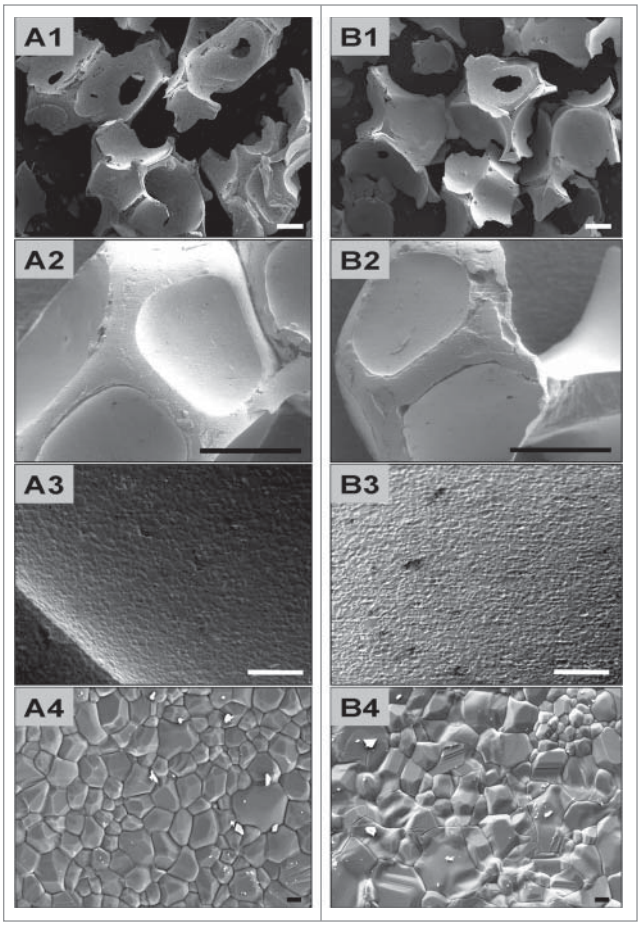

Figure 1. shows SEM pictures of the analyzed bone substitute granules. **A1–3** show the properties of BoneCeramic (BC) with granule sizes between 500–1000 μm, while **B1–3** show the characteristics of BoneCeramic (BC) with granule sizes between 400–700 μm. Note the differences in granule sizes between BoneCeramic 500–1000 μm and 400–700 μm (A1 and B1), while no differences were observable in the other physical properties, such as granule shape (A2 and B2), surface texture and pore distribution (A3 and B3) (A1 and B1: 25x magnification, scale bar = 1 mm; A2 and B2: 200x magnification, scale bar = 200 μm; A3 and B3: 1000x magnification, scale bar = 20 μm).

Tissue reaction to BoneCeramic® 400–700 μm. On day 3 after implantation, a mixture of fibrin and connective tissue fibers as well as large numbers of mononuclear cells of the monocyte/macrophage lineage and granulocytes were found in the implantation bed of the bone substitute material with the smaller granule size,

namely BoneCeramic® 400–700 μm (BC 400–700) (**Fig. 2** B1). Small vessels started to grow toward the implantation bed, which showed no signs of vascularization at this time point (**Fig. 2** B1). No multinucleated giant cells were observable.

On day 10 after implantation, the BC 400–700 granules were embedded within a cell- and vessel-rich connective tissue including different mononuclear cells such as fibroblasts, lymphocytes and monocytes/macrophages (**Fig. 2** B2). Furthermore, small numbers of mainly TRAP-positive multinucleated giant cells were located at the surface of the bone substitute granules besides large numbers of mononuclear cells (**Fig. 2** B2 and 3 B1). On days 15, 30 and 60 after implantation, the granulation tissue with the previously described cellular composition was still observed within the implantation beds of the BC 400–700 (**Fig. 2** B3-5). A maturation of the vessels in comparison to day 10 was seen, starting with day 15, and this condition persisted up to day 60 (**Fig. 2** B3-5). At day 15, moderate numbers of TRAP-positive multinucleated cells were found at the material-tissue-interfaces, comparable to those at day 10, while an increase in their number and also of their TRAP-expression was visible at day 30 and day 60 after implantation (**Fig. 3** B2–4). Within this time span, large portions of the surface area of the BC 400–700 granules were still covered by mononuclear cells that often showed signs of TRAP expression (**Fig. 3** B2-4).

Tissue reaction toward BoneCeramic® 500–1000 μm. On day 3 after implantation, a loose network of matrix fibers and mononuclear cells (cells of the monocyte/macrophage line, granulocytes, lymphocytes and fibroblasts) was observed at the surface of the granules within the implantation beds of the bone substitute material with the larger granule size, BoneCeramic® 500–1000 μm (BC 500–1000) (**Fig. 2** A1). At this time point, no vessels or multinucleated giant cells were detected. On day 10 after implantation, the intergranular spaces of the BC 500–1000 granules were filled by a cell-rich connective tissue consisting of lymphocytes, granulocytes and cells of the monocyte/macrophage line (**Fig. 2** A2). In this group, moderate numbers of multinucleated giant cells, a small number of which showed signs of TRAP expression (**Fig. 3** A1), were located at the biomaterial-tissue interfaces in addition to large numbers of mononuclear cells (**Fig. 2** A2), of which a moderate number were TRAP-positive (**Fig. 3** A1). Furthermore, a small number of vessels was also detectable within the intergranular connective tissue at the periphery, which began to grow into the central regions of the implantation bed (**Fig. 2** A2). At days 15, 30 and 60 after implantation, the intergranular spaces of the granules still contained the above-described connective tissue (**Fig. 2** A3-5). At these time points, a large number of vessels was detectable, with lumina visibly larger than on day 10 (**Fig. 2** A3-5). Within this time span, the number of multinucleated giant cells and the fractions of their TRAP-positive and TRAP-negative subforms did not change compared to those at day 10 after implantation (**Fig. 3** A2-4). High numbers of mononuclear cells were still visible at the surfaces of the

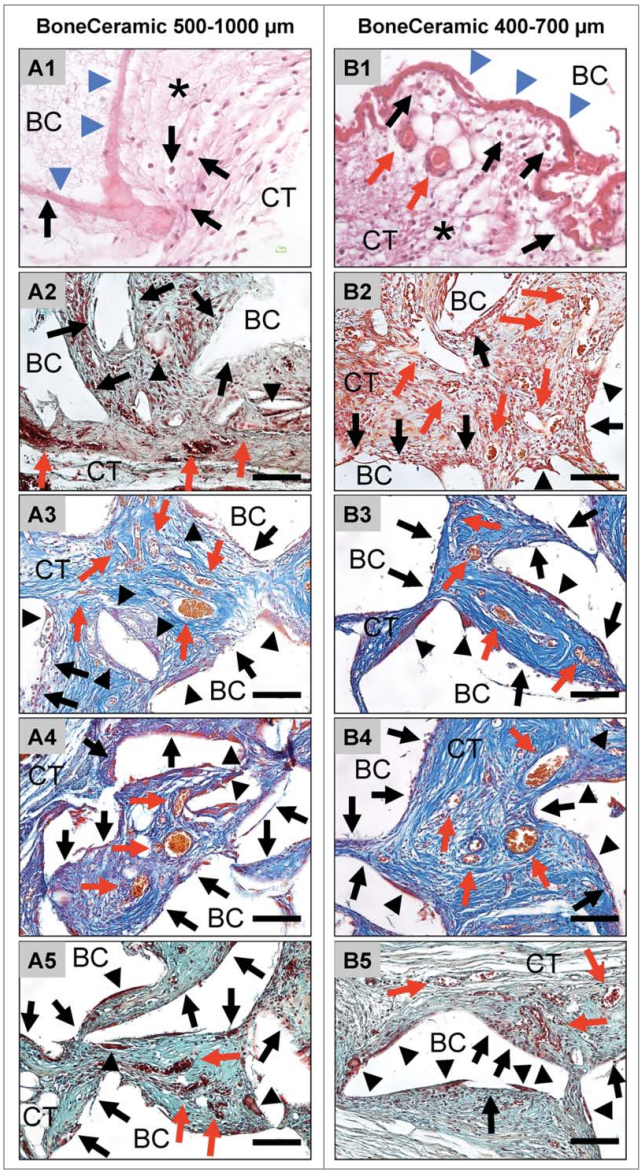

Figure 2. shows the tissue reactions as well as the vascularization pattern of the 2 analyzed bone substitute granule types, BoneCeramic 500–1000 μm and BoneCeramic 400–700 μm. **A1** and **B1**: On day 3, a surface layer composed of fibrin and connective tissue fibers (blue arrows) was observed on the surface of both materials, while the granules (BC) were embedded within an fiber-rich and loose connective tissue (CT) (H&E-staining, 400x magnification, scale bars = 10 μm). **A2 – A3** and **B2 – B3**: On days 10 and 15, the interspaces of both bone substitute granules (BM) were filled up by a cell- and vessel-rich (red arrows) connective tissue (CT). At the surfaces of both granule sizes mainly mononuclear cells (black arrows) were detectable beside low numbers of multinucleated giant cells (arrow heads) (A2 and B2: Movat Pentachrome-stainings; A3 and B3: Azan-stainings; 400x magnification, scale bars = 10 μm). **A4 – A5** and **B4 – B5**: On days 30 and 60 both granule sizes of the bone substitute (BC) were still surrounded by a cell- and vessel-rich (red arrows) connective tissue (CT). Also primarily mononuclear cells (black arrows) were found at the surfaces of both materials, while increased numbers of multinucleated giant cells (arrow heads) were found in the implantation beds of BoneCeramic 400–700 μm (B4 and B5) compared with those of BoneCeramic 500–1000 μm (A4 – A5) (A4 and B4: Azan-staining; A3 and B3: Movat Pentachrome-staning; 400x magnification, scale bars = 10 μm).

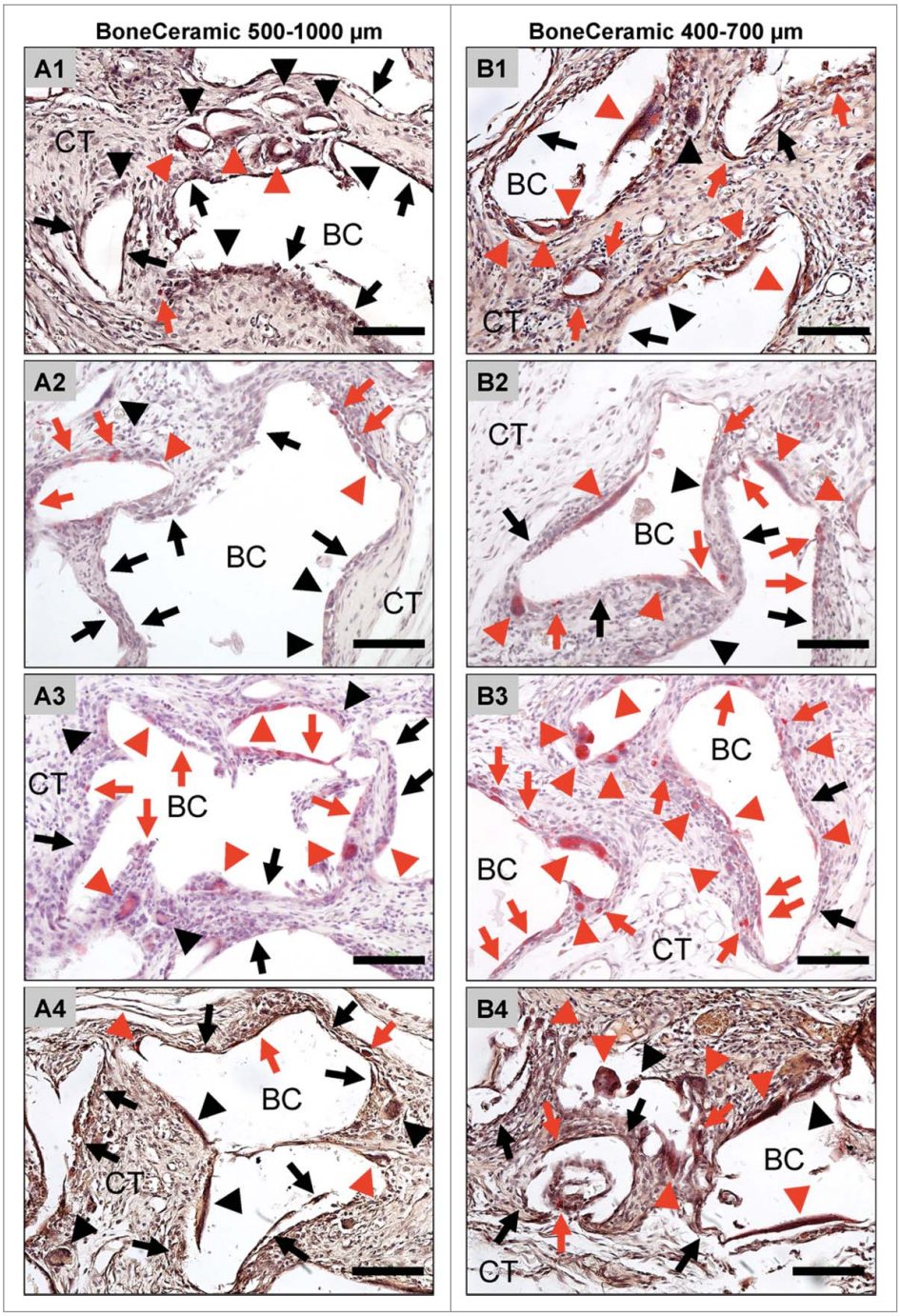

Figure 3. shows exemplary pictures of the TRAP-activity of the material-associated multinucleated giant cells adjacent to the bone substitute granules of BoneCeramic 500–1000 µm (**A1 – A4**) and BoneCeramic 400–700 µm (**B1 – B4**) on days 10 (**A1 and B1**), 15 (**A2 and B2**), 30 (**A3 and B3**) and 60 (**A4 and B4**) after implantation (TRAP-staining, 200x magnification, scale bars = 100 µm).

granules at these time points, and they often showed signs of TRAP expression (**Fig. 3** A2-4).

Quantitative histomorphometry

Histomorphometry of implant bed vascularization. The histomorphometrical measurements of vascularization revealed no significant differences between the 2 study groups and the control group on day 3 after implantation (**Fig. 4A and B**). The implantation beds of both granule types did not contain any vessels, while the defect area of the control group showed only minor vascularization (7.94 ± 1.95 vessels/mm^2 and 0.06 ± 0.01%) (**Fig. 4A and B**).

On day 10 after implantation, the implantation beds of BC 400–700 showed significantly higher vascularization values, both in number of vessels (39.56 ± 5.96 vessels/mm^2) (*p > 0.05) and in percent vascularization (2.20 ± 0.43%) (**p > 0.01), than those of BC 500–1000 (21.68 ± 4.36 vessels/mm^2 and 1.46 ± 0.31%) (**Fig. 4A and B**). Furthermore, only the vessel density in the BC 400–700 group was significantly higher than that of the control group (9.13 ± 0.98 vessels/mm^2) (***p > 0.001) (**Fig. 4A**). The vascularization percentages in the groups of both granule types were significantly larger than in the control group (0.08 ± 0.02%) (***p > 0.001) (**Fig. 4B**). At this time point, the intra-individual analyses revealed significant increases in both vascularization parameters relative to day 3 only in the groups of the bone substitute materials (•• p > 0.01 / ••• p > 0.001) (**Fig. 4A and B**).

Starting with day 15 and until day 60 after implantation, no significant differences between the vascularization parameters of the groups of bone substitute material were found (**Fig. 4A and B**). Values of 44.27 ± 5.82 vessels/mm^2 and 2.27 ± 0.13% were quantified for BC 500–1000, comparable to the values obtained for BC 400–700 (42.81 ± 7.12 vessels/mm^2 and 2.06 ± 0.22%) at day 15 after implantation (**Fig. 4A and B**). The vascularization values in both biomaterial groups were significantly higher than the values of the control group (9.95 ± 1.69 vessels/mm^2 and 0.24 ± 0.10%) at this time point (***p > 0.001) (**Fig. 4A and B**). Intraindividual differences compared to the previous time point were only found in the group of the BC 500–100 in both vascularization parameters (••p > 0.01) (**Fig. 4A and B**).

At day 30 after implantation, no significant differences were measured in the vascularization parameters in the groups of BC 500–1000 (42.41 ± 6.82 vessels/mm^2 and 1.87 ± 0.15%) and

BC 400–700 (40.48 ± 11.18 vessels/mm^2 and 1.82 ± 0.18%) (**Fig. 4A and B**). At this time point, significant differences were still found between the vascularization parameters of these both groups and those of the control group (10.03 ± 0.91 vessels/mm^2 and 0.29 ± 0.06%) (***p > 0.001) (**Fig. 4A and B**). However, no intraindividual differences in any of the 3 groups compared to the respective values at the former time point were measured (**Fig. 4A and B**).

On day 60 after implantation, no statistical significance was found between the values of the vascularization parameters of the groups of BC 500–1000 (39.37 ± 4.04 vessels/mm^2 and 1.96 ± 0.21%) and BC 400–700 (42.83 ± 10.53 vessels/mm^2 and 1.88 ± 0.28%) (**Fig. 4A and B**). The values of both vascularization parameters were significantly lower in the control group (17.69 ± 0.49 vessels/mm^2 and 1.11 ± 0.16%) than in either material group (***p > 0.001) (**Fig. 4A and B**). No intraindividual differences were found in either group of the bone substitute material, while a significant increase of the percent vascularization was measured in the control group (••p > 0.01) (**Fig. 4A and B**).

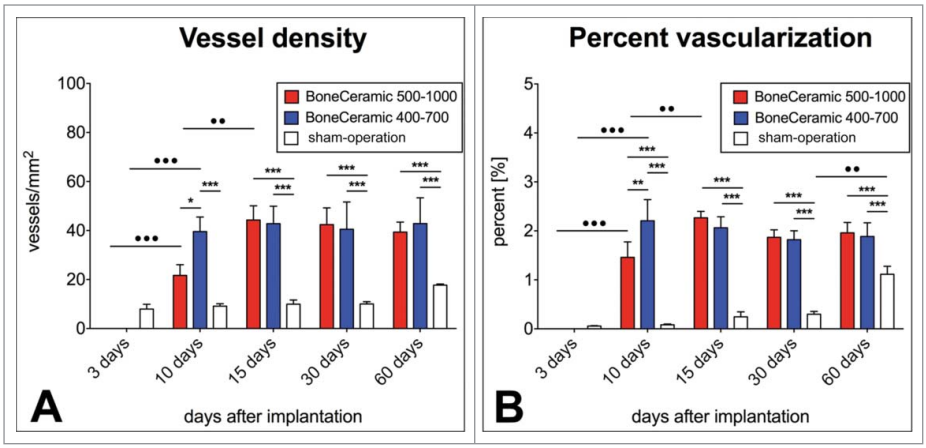

Figure 4. shows the results of the histomorphometrical vascularization analysis of the implantation beds of the 2 bone substitute granule types compared with the control group. (**A**) Vessel density; (**B**) percent vascularization (*/**/*** = inter-individual statistical significances, •/••/••• = intra-individual statistical significances).

Histomorphometry of giant cell activity

Total number of multinucleated giant cells. On day 3 after implantation, no multinucleated giant cells (MNGCs) were observable within the implantation beds of either of the biphasic bone substitute materials (**Fig. 5**). Starting on day 10 after implantation, comparable quantities of MNGCs, which were significantly higher as compared with the values at day 3 (•••p > 0.001), were measured in the groups of BC 400–700 (16.62 ± 2.34 MNGCs/mm^2) and BC 500–1000 (12.07 ± 1.64 MNGCs/mm^2) (**Fig. 5A**).

On day 15 after implantation, there was still no significant difference in the number of MNGCs in the implantation beds of BC 400–700 (19.29 ± 1.03 MNGCs/mm^2) and BC 500–1000 (15.41 ± 2.21 MNGCs/mm^2), and also no significant intraindividual differences were observed compared to day 10 (**Fig. 5A**).

Starting on day 30 after implantation, the number of MNGCs in the BC 400–700 implantation beds (28.25 ± 5.15 MNGCs/mm^2) was significantly larger than in the group of BC 500–1000 (16.51 ± 1.31 MNGCs/mm^2) (*** p > 0.001) (**Fig. 5A**). Moreover, an intraindividual increase was found in the group of BC 400–700 (•••p > 0.001) compared to the numbers at day 15, while the values were on a comparable level in the study group of BC 500–1000 (**Fig. 5A**).

On day 60 after implantation, significantly larger numbers of MNGCs were still detectable in the implantation beds of BC 400–700 (27.83 ± 1.89 MNGCs/mm^2) compared to the numbers in the BC 500–1000 implantation beds (16.79 ± 1.94 MNGCs/mm^2) (***p > 0.001) (**Fig. 5A**). No intraindividual differences were found in either study groups compared to the values of the previous time point (**Fig. 5A**).

Amount of TRAP-positive multinucleated giant cells. Starting on day 10 after implantation, comparable numbers of TRAP-positive multinucleated giant cells (MNGCs) were found in the BC 500–1000 implantation beds (5.42 ± 0.66 TRAP-positive MNGCs/mm^2) and the BC 400–700 implantation beds (6.66 ± 1.42 TRAP-positive MNGCs/mm^2), these being significantly higher compared to the values at day 3 (••p > 0.01 / •••p > 0.001) (**Fig. 5B**).

On day 15 after implantation, a significant difference (* p > 0.05) between the numbers of the TRAP-positive MNGCs in the BC 500–1000 implantation beds (5.37 ± 0.81 TRAP-positive MNGCs/mm^2) and the BC 400–700 implantation beds (9.68 ± 1.74 TRAP-positive MNGCs/mm^2) was observed, but the intraindividual differences compared to the previous time point were insignificant (**Fig. 5B**).

On day 30 after implantation, the number of TRAP-positive MNGCs was also significantly higher (*** p > 0.001) in the BC 400–700 implantation beds (16.13 ± 3.24 TRAP-positive MNGCs/mm^2) compared with those in the BC 500–1000 implantation beds (6.91 ± 0.78 TRAP-positive MNGCs/mm^2) (**Fig. 5B**). The values in the BC 400–700 beds were significantly larger than on day 15 (•••p > 0.001) (**Fig. 5B**), but there was no significant change in the BC 500–1000 implantation beds (**Fig. 5B**).

On day 60 after implantation, the number of TRAP-positive MNGCs was significantly higher (***p > 0.001) in the BC 400–700 implantation beds (17.50 ± 1.87 TRAP-positive MNGCs/mm^2) than in the BC 500–1000 group implantation beds (7.48 ± 0.95 TRAP-positive MNGCs/mm^2), but neither group demonstrated a significant increase from day 30 (**Fig. 5B**).

Amount of TRAP-negative multinucleated giant cells. On day 10, comparable amounts of TRAP-negative multinucleated giant cells (MNGCs) were found in the BC 500–1000 implantation

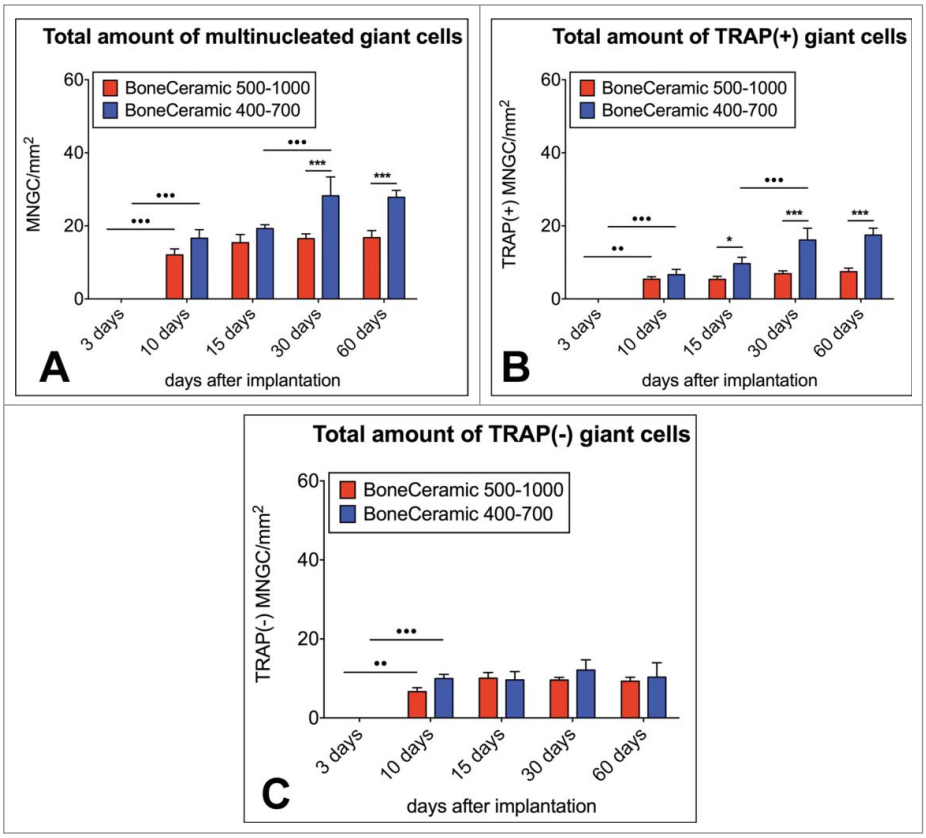

Figure 5. shows the results of the histomorphometrical giant cell analysis within the implantation beds of the 2 bone substitute typess considering the different cellular activity conditions, including the total number of material-related multinucleated giant cells (**A**) as well as the TRAP-positive (**B**) and the TRAP-negative multinucleated giant cells (**C**) (*/**/*** = inter-individual statistical significances, •/••/••• = intra-individual statistical significances).

beds (6.65 ± 1.01 TRAP-negative MNGCs/mm^2) and the BC 400–700 implantation beds (9.96 ± 1.08 TRAP-negative MNGCs/mm^2) (**Fig. 5C**). Both of these numbers were significantly higher than the values on day 3 after implantation (••p > 0.01 / •••p > 0.001) (**Fig. 5C**).

On day 15 after implantation, there was no significant change since day 10, as the implantation beds of BC 500–1000 (10.04 ± 1.45 TRAP-negative MNGCs/mm^2) and BC 400–700 (9.61 ± 2.13 TRAP-negative MNGCs/mm^2) again showed similar values (**Fig. 5C**)

These trends were also observed on day 30 after implantation, when the BC 500–1000 implantation beds contained 9.59 ± 0.68 TRAP-negative MNGCs/mm^2 and the BC 400–700 implantation beds showed 12.12 ± 2.57 TRAP-negative MNGCs/mm^2, and on day 60 after implantation, when the respective numbers for the BC 500–1000 and BC 400–700 beds were 9.31 ± 0.99 and 10.34 ± 3.63 TRAP-negative MNGCs/mm^2 (**Fig. 5C**).

Degradation analysis using transmission electron microscopy (TEM)

Transmission electron microscopy analysis (TEM) showed no differences between the involvement of mono- and multinucleated giant cells in the 2 groups, nor were differences found in the (sub-) cellular structure or the cell organelles. Thus, the following results applied to both groups.

On TEM both mono- and multinucleated cells were located at the surfaces of the bone substitute material granules on day 15 after implantation (**Fig. 6 and** 7), exhibiting a tightly packed cytoplasm containing mainly cell organelles such as mitochondria, many different vacuoles with homogeneous contents and a ramified rough endoplasmic reticulum (rER) (**Fig. 6B, C, 7B and C**). Vacuoles were also found within their cytoplasm in the vicinity of the previously mentioned vacuoles that contained fragments of the bone substitute materials (**Fig. 6B, C** and 7A). The multinucleated giant cells were adherent to the surfaces of the bone substitute granules via podosomal branches (**Fig. 7B and D**) that appeared to demarcate an extracellular compartment between the material-adherent pole of the giant cells and the material surfaces that were filled up with homogenous content (**Fig. 7B–D**).

Quantitative analysis of phagocytosed particles using TEM. The histomorphometrical measurements showed that the phagocytosed bone substitute particles within the mononuclear cells had comparable sizes in the group of BC 500–1000 (0.63 ± 0.34 μm) and BC 400–700 (0.58 ± 0.42 μm) (**Fig. 8**).

Discussion

Physical characteristics of bone substitute materials such as porosity, surface structure and shape have been identified as regulators of the tissue reaction, material degradation, and not least the regenerative potential of synthetic bone substitutes.[8-13] Granule size is also believed to have a major influence on the successful application of bone substitute materials, as it is supposed to regulate the degradability of bone substitutes.[8] However, until now no consensus has been found concerning this material factor. Some study results have shown that the application of small-sized granules up to 100 μm seems to be preferable for bone regeneration in contrast to granules with diameters above.[14-19,24] In contrast, further results show that granules with higher diameters ranging from 100 – 1000 μm allow a higher level of regeneration.[28-30] It has been suggested that material granules should have pores of sizes between 40 – 100 μm for optimal integration

and the best level of regeneration, which can also be obtained for granules of sizes larger than 380 μm.[40,41]

As a result of this lack of knowledge regarding this material factor, the present study was conducted to analyze the influence of the granule size of synthetic biphasic bone substitute materials on the inflammatory tissue reaction using an established subcutaneous implantation model in Wistar rats for up to 60 d.[6,14, 32-37] In addition, previously described histological and histomorphometrical methods were also employed. Therefore, 2 granule sizes of a biphasic bone substitute material, BoneCeramic® 500–1000 μm (BC 500–1000) and BoneCeramic® 400–700 μm (BC 400–700), were used. All other material characteristics such as chemical composition as well as granule shape, surface texture and pore distribution were initially shown to be equal.

The present *in vivo* analysis initially showed that mainly mononuclear cells such as macrophages and only low numbers of multinucleated giant cells were found within the implantation beds of both biphasic materials. This result is surprising as the numbers of the multinucleated giant cells were lower compared to other synthetic bone substitute materials based on pure calcium phosphates, i.e., pure HA and pure β-TCP, and also in case of another biphasic material with the same chemical biphasic composition of 60% HA and 40% β-TCP.[6] Interestingly, the values of MNGCs are comparable to the values found within the implantation beds of a low temperature-sintered xenogeneic bone substitute material (Bio-Oss®).[37] This biomaterial represents purified bovine extracellular calcified bone matrix and is regarded as having physicochemical properties similar to those of autologous bone grafts, which are considered to be the "gold standard" for bone regeneration.[1,2,42] As it has been shown that the resorbability of this xenogeneic material is delayed, the presented results raise the question of whether the low numbers of multinucleated giant cells in the case of the analyzed biphasic materials also lead to a low rate of degradation and therefore a prolonged material standing time.[37,43] However, the increase of the numbers of MNGCs and especially of their TRAP-positive subforms at the end of the study period in the case of the small-sized BC 400–700 are interesting. As also shown by the transmission electron microscopy (TEM) analysis in the present study the multinucleated giant cells are involved in the degradation of both materials and, thus, the increase in their

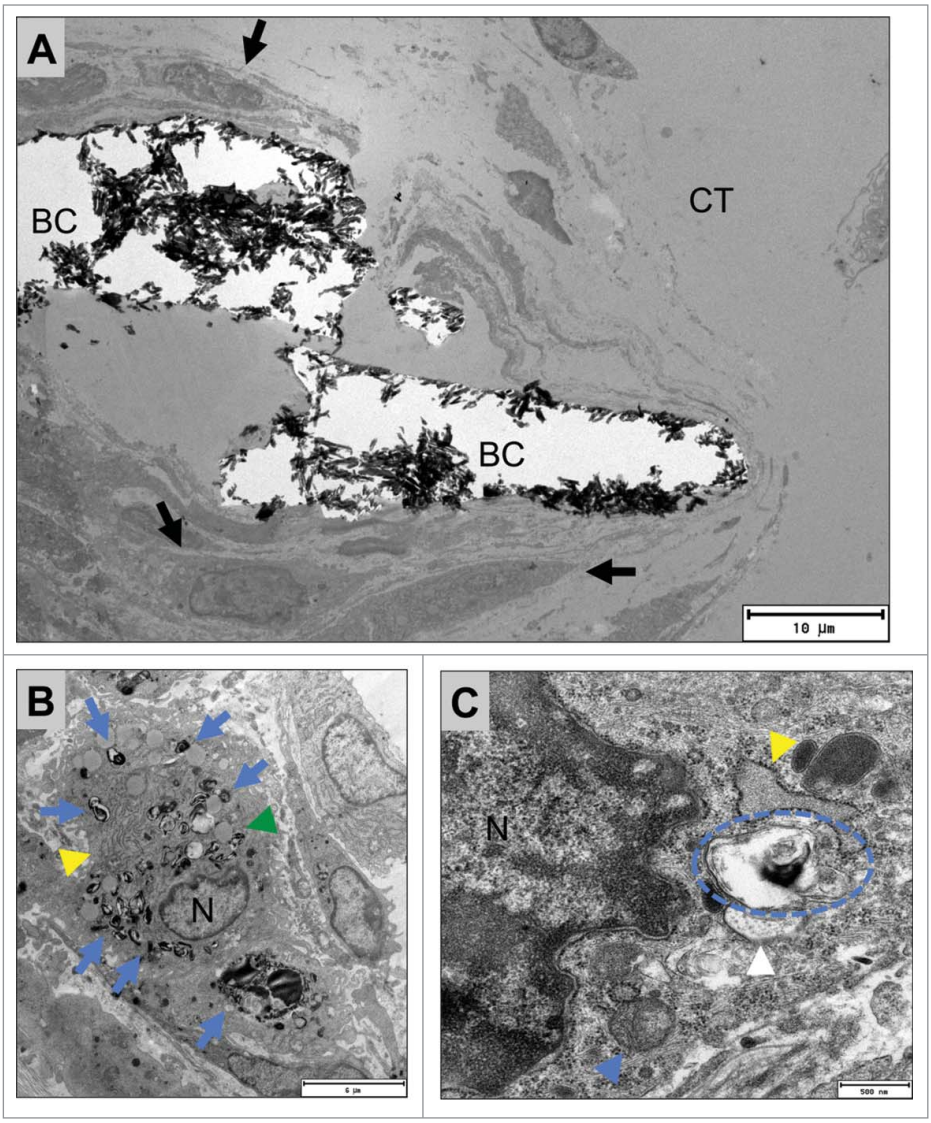

Figure 6. shows TEM images of the mononuclear cells involved in the tissue reactions to the BoneCeramic 400–700 μm (BC) bone substitute on day 15 after implantation. (**A**) Shows an overview of the implantation bed of BoneCeramic 400–700 μm granules (BC) within the subcutaneous connective tissue (CT) of the CD-1 mouse. At the surfaces of the granules, primarily mononuclear cells (black arrows) were detectable (690x magnification, scale bar = 10 μm). (**B**) Shows a material-related mononuclear cell that has vacuoles containing phagocytosed bone substitute material fragments (blue arrows). These vacuoles were regularly found within the cytoplasm of the cell in the direct vicinity of cisterns of the rough endoplasmic reticulum (yellow arrow head) as well as vacuoles with electron-dense contents (green arrow head) (N = nucleus) (1900x magnification, scale bar = 6 μm). (**C**) Shows the cytoplasm of the material-adherent phagocytosing mononuclear cell at a higher magnification. Vacuoles containing phagocytosed material fragments (blue dashed line) were regularly observed within the direct vicinity of cisterns of the rough endoplasmic reticulum (yellow arrow head) as well as other cell organelles that seemed to be involved in the process of active phagocytosis, such as mitochondria (blue arrow head) (N= nucleus). Interestingly, a vesicle (white arrow head) seemed to fuse with the vesicle containing the material fragment (13000x magnification, scale bar = 500 nm).

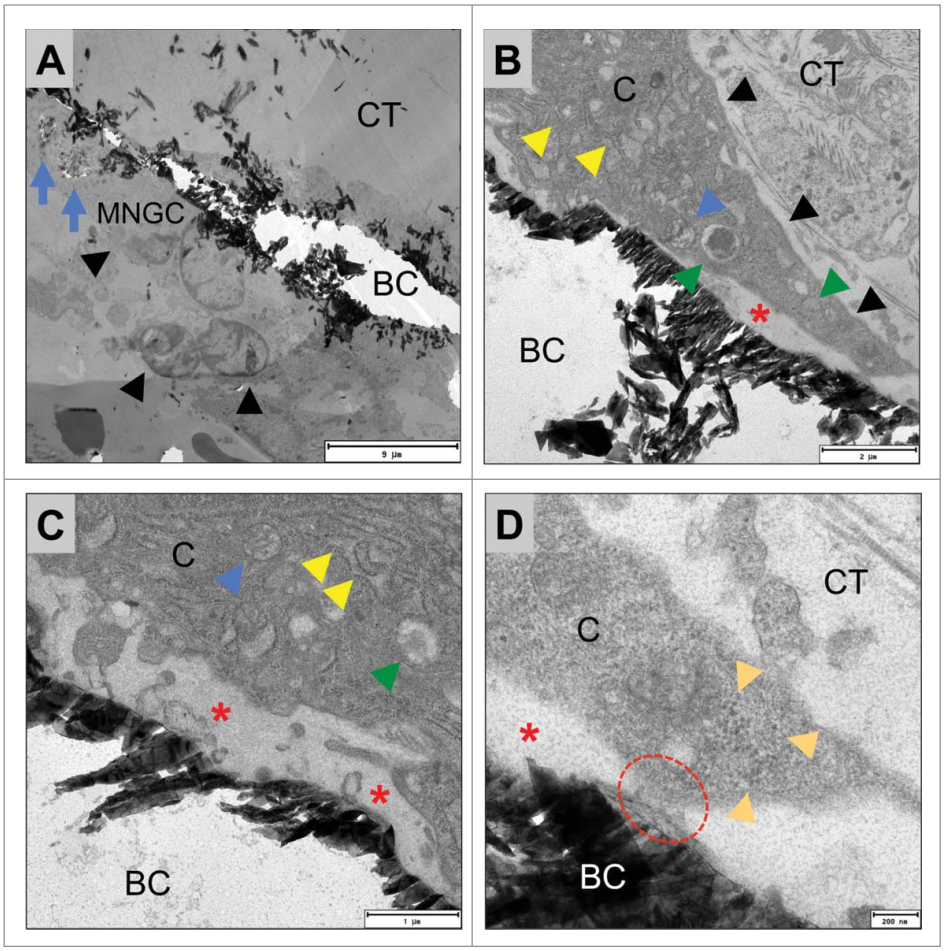

Figure 7. shows TEM pictures of the multinucleated giant cells adherent to the surfaces of BoneCeramic 500–1000 μm granules (BC) within the subcutaneous connective tissue (CT) of the CD-1 mouse on day 15 after implantation. (**A**) shows an overview of a material-adherent multinucleated giant cell (MNGC, black arrow heads) at the surface of the BoneCeramic 500–1000 μm (BC) that has invaginated material fragments (blue arrows) (1200x magnification, scale bar = 9 μm). (**B**) and (**C**) show a multinucleated giant cell (black arrow heads) adherent to a BC 500–1000 granule surface (BC). Within their cytoplasm (CP) mitochondria (blue arrow heads), many cisterns of the rough endoplasmic reticulum (rER, red arrow head) and different vesicles (green arrow heads) were found. Furthermore, a zone demarcated by the material surface and the cell membrane of the giant cell (red asterisks) was found that did not contain cell organelles but rather electron-dense content (**B**) 4800x magnification, scale bar = 2 μm; (**C**): 9300x magnification, scale bar = 1 μm). (**D**) Shows the adherent podosome-like cell branch (read dashed line) of the multinucleated giant cell (C = cytoplasm) at the surface of the bone substitute granule (BC) that seems to separate the demarcation zone (red asterisk) from the surrounding connective tissue (CT). Furthermore, a bundle of intracellular intermediate filaments were found near the cell branch (orange arrow heads) (23000x magnification, scale bar = 200 nm).

numbers seems to indicate that the small granules of the BC 400–700 could become degraded faster than the granules of the BC 500–1000. Unfortunately, no histomorphometrical measurement of the particle size phagocytosed by the multinucleated giant cells was possible. However, it is suggested that the particle size, which could be invaginated by multinucleated cells, is greater because of the higher „reserves" of membranes involved in the process of phagocytosis.[44]

This phenomenon might be a result of the fact that the overall implant surface area of the material with smaller granule size especially at the later time point is higher compared to that with the larger granule size, although equal weights of the 2 materials were implanted. As a consequence, the larger surface area on the one hand could have promoted the induction of macrophage fusion compared to the granules with larger diameters. Additionally, the extent of dissolution, i.e., the non cell-related degradation, of the 2 biphasic bone substitutes may have been different. Thus, the small-sized granules could have been subject to a higher extent of dissolution, which could have resulted in a faster "achievement" of a granule size that promotes the induction of macrophage fusion.

Interestingly, the histomorphometrical analysis based on TEM additionally showed that the mononuclear cells involved in the tissue reactions to the bone substitute materials were able to phagocytose particles with a mean diameter of approximately 0.6 μm and a maximal diameter of 2 μm, without significant differences between both groups. This could be because both granule types were prepared by the same manufacturing process and from the same precursor material, and thus their "subunits" have the same size and structure. This means that the solution of fragments by the phagocytosing cells could be similar for these materials. Furthermore, these results are fully in line with other studies showing that macrophages are able to phagocytose particles in the range of 0.7 – 3.2 μm.[44-46] Thus, the presented data show that the degradation rates of both granules of the bone substitute seem mainly to be based on the (numbers of) multinucleated giant cells.

However, based on these data the question arises whether a faster degradation of small-sized bone substitute granules is supportive of the process of bone regeneration. Thus, implantation in bone tissue using a special preclinical operation model could permit clarification of this question.

Additionally, the question also arises concerning which properties of the analyzed bone substitute materials could have induced tissue reactions similar to those of the xenogeneic bone substitute material. In this context the initial SEM analysis of the material characteristics showed that the granules of both bone substitutes had a relatively smooth surface topography. Generally, this material factor has been described as a key factor for the

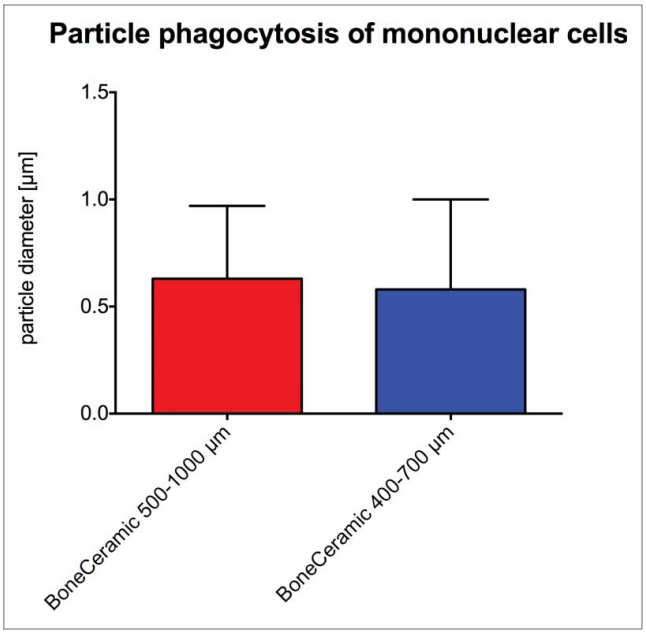

Figure 8. shows the results of the histomorphometrical measurements of the particle sizes phagocytosed by mononuclear cells in the cases of both granule sizes of the bone substitute material.

tissue reaction to a biomaterial and a smooth biomaterial surface topography of a biomaterial as also observed in case of the analyzed bone substitutes has impact on the severity of the foreign body reaction involving mononuclear cells such as macrophages, rather than multinucleated giant cells.[13,47-49] Thus, it is presumed that even this material factor could have determined the observed tissue reactions, that are comparable to those observed in the xenogeneic biomaterial.

A further interesting result was the significantly higher implant bed vascularization in the group of the small-sized bone substitute of the BC 400–700 at day 10 after implantation, while after that time point no further differences between the 2 study groups were found. As no correlation between the presence of multinucleated giant cells and vascularization in the case of the analyzed biphasic bone substitute was found, in contrast to the vascularization mechanisms of other bone substitutes previously analyzed by our group, these quantitative results lead to the conclusion that mononuclear cells such as macrophages were also mainly involved in the vascularization processes of both biphasic bone substitute materials.[6,14,33-35,37] In this context, especially macrophages have been shown to be involved in the implant bed vascularization via their secretion of angiogenic factors such as the vascular endothelial growth factor (VEGF), which is a potent inducer of vascularization.[50,51] Thus, the early high vascularization in the case of the small-sized granules (BC 400–700) could also be related to the induction of a higher expression of VEGF in these mononuclear cells. This data became substantiated by other study results indicating that even material granules with smaller diameters can evoke higher levels of pro-inflammatory enzymes and also VEGF from macrophages, especially in the early phase after implantation.[26] Based on these data it could be concluded that the small-sized bone substitute granules might also induce a higher or faster level of bone tissue growth, as VEGF also stimulates the proliferation and differentiation of osteoblasts in a dose-dependent manner.[51,52] However, further studies have to be conducted using also bone implantation models to clarify this issue.

Finally, the TEM analysis showed that both the mononuclear cells as well as the multinucleated giant cells were involved in the degradation of both granule sizes of the bone substitute material by phagocytosis of material fragments, which substantiates further evidence for the differentiation of this material-induced multinucleated cell type. Cell organelles that are known to be involved in the process of phagocytosis, including the ramified rough endoplasmic reticulum (rER), and vacuoles with electron-dense contents near the phagocytosis vacuoles reminiscent of lysosomes or other vacuoles with lytic enzymes, have also been detected within both cell types.[53,54] Additionally, these data substantiate further evidence for the differentiation of the material-induced multinucleated cell type, which has been assigned to the cell type of the foreign body giant cell, as no ruffled border was detectable.[55] The ruffled border is a crucial subcellular element for the functionality of the osteoclast as it enables resorption of fragments of the bone matrix (collagen and calcium) after its dissolution in an acid microenvironment and its transport via transcytosis. Thus, the osteoclast is also a "phagocytosing" cell type, but no description of the phagocytosis of „greater" fragments of bone substitutes or foreign bodies has been described in these cells in contrast to foreign body giant cells.[56-58] Thus, the presented invagination of larger synthetic material fragments in combination with the absence of the ruffled border again lead to the conclusion that the observed material-adherent multinucleated giant cells are indeed foreign body giant cells. However, these results ultimately support the hypothesis that this biomaterial-induced multinuclear cell type "uses" similar mechanisms to dissolve the calcium phosphate content of the bone substitute materials, such as a subcellular compartment within an acid microenvironment comparable to the clear zone and even TRAP enzymes, while not being a cell of the osteoclast line with all its phenotypic characteristics such as the ruffled border or the calcitonin receptor.[13,53-61]

Altogether, based on the presented data it appears that a foreign body reaction to biomaterials or bone substitute materials could also be executed mainly by mononuclear cells in the same way as multinucleated giant cells, characterized by the ability to degrade a biomaterial and phagocytose material fragments. Thus, the results revealed that synthetic bone substitute materials such as the analyzed biphasic material can induce tissue reactions similar to those of some xenogeneic materials. Furthermore, the results show that the granule size seems to have impact only on early implant bed vascularization and also on the induction of MNGCs in the late phase of the tissue reaction, which could cause a different degradation time for small-sized granules compared to the larger granules. Moreover, the results indicate that granule size did not alter the phagocytic capacity of mononuclear cells, as the underlying material structure generated by the (common) production processes seems to yield phagocytosis subunits

with similar sizes, no matter what size the macrogranules have originally. Finally, the investigation substantiates the differentiation of material-induced MNGCs, which are of the foreign body giant cell type.

Disclosure of Potential Conflicts of Interest

No potential conflicts of interest were disclosed.

Acknowledgment

The authors would like to thank Ms. Ulrike Hilbig and Mr. Mykhaylo Reshetnykov for their technical assistance.

Funding

This research was funded by the ITI International Team for Implantology (ITI Research Grant No. 601_2008).

References

1. Damien CJ, Parsons JR. Bone graft and bone graft substitutes: a review of current technology and applications. J Appl Biomater 1991; 2(3):187-208; PMID:10149083; http://dx.doi.org/10.1002/jab.770020307
2. Nandi SK, Roy S, Mukherjee P, Kundu B, De DK, Basu D. Orthopaedic applications of bone graft & graft substitutes: a review. Indian J. Med. Res. 2010; 132:15-30
3. Kamitakahara M, Ohtsuki C, Miyazaki T. Review paper: behavior of ceramic biomaterials derived from tricalcium phosphate in physiological condition. J Biomater Appl 2008; 23(3):197-212; PMID:18996965; http://dx.doi.org/10.1177/0885328208096798
4. Blokhuis TJ, Termaat MF, den Boer FC, Patka P, Bakker FC, Haarman HJ. Properties of calcium phosphate ceramics in relation to their in vivo behavior. J Trauma 2000; 48(1):179-86; PMID:10647592; http://dx.doi.org/10.1097/00005373-200001000-00037
5. Lobo SE, Livingston Arinzeh T. Biphasic calcium phosphate ceramics for bone regeneration and tissue engineering applications. Materials 2010; 3(2):815-26; PMID:24710095; http://dx.doi.org/10.3390/ma3020815
6. Ghanaati S, Barbeck M, Detsch R, Deisinger U, Hilbig U, Rausch V, Sader R, Unger RE, Ziegler G, Kirkpatrick CJ. The chemical composition of synthetic bone substitutes influences tissue reactions in vivo: histological and histomorphometrical analysis of the cellular inflammatory response to hydroxyapatite, beta-tricalcium phosphate and biphasic calcium phosphate ceramics. Biomed Mater 2012; 7(1):015005; PMID:22287541; http://dx.doi.org/10.1088/1748-6041/7/1/015005
7. Daculsi G, LeGeros RZ, Nery E, Lynch K, Kerebel B. Transformation of biphasic calcium phosphate ceramics in vivo: ultrastructural and physicochemical characterization. J Biomed Mater Res 1989; 23(8):883-94; PMID:2777831; http://dx.doi.org/10.1002/jbm.820230806
8. Hing KA. Bioceramic bone graft substitutes: influence of porosity and chemistry. Int J Appl Ceram Tech 2005; 2:184-99; PMID:16378638; http://dx.doi.org/10.1111/j.1744-7402.2005.02020.x
9. Lu J, Descamps M, Dejou J, Koubi G, Hardouin P, Lemaitre J, Proust JP. The biodegradation mechanism of calcium phosphate biomaterials in bone. J Biomed Mater Res 2002; 63(4):408-12; PMID:12115748; http://dx.doi.org/10.1002/jbm.10259
10. Kasten P, Beyen I, Niemeyer P, Luginbuhl R, Bohner M, Richter W. Porosity and pore size of β-tricalcium phosphate scaffold can influence protein production and osteogenic differentiation of human mesenchymal stem cells: an in vitro and in vivo study. Acta Biomater 2008; 4(6):1904-15; PMID:18571999; http://dx.doi.org/10.1016/j.actbio.2008.05.017
11. Boyan BD, Bonewald LF, Paschalis EP, Lohmann CH, Rosser J, Cochran DL, Dean DD, Schwartz Z, Boskey AL. Osteoblast-mediated mineral deposition in culture is dependent on surface microtopography. Calcif Tissue Int 2002; 71(6):519-29; PMID:12232675; http://dx.doi.org/10.1007/s00223-001-1114-y
12. von Doernberg MC, von Rechenberg B, Bohner M, Grünenfelder S, van Lenthe GH, Müller R, Gasser B, Mathys R, Baroud G, Auer J. In vivo behavior of calcium phosphate scaffolds with four different pore sizes. Biomaterials 2006; 27(30):5186-98; PMID:16790273; http://dx.doi.org/10.1016/j.biomaterials.2006.05.051
13. Anderson JM, Rodriguez A, Chang DT. Foreign body reaction to biomaterials. Semin Immunol 2008; 20(2):86-100; PMID:18162407; http://dx.doi.org/10.1016/j.smim.2007.11.004
14. Ghanaati S, Barbeck M, Orth C, Willershausen I, Thimm BW, Hoffmann C, Rasic A, Sader RA, Unger RE, Peters F, Kirkpatrick CJ. Influence of β-tricalcium phosphate granule size and morphology on tissue reaction in vivo. Acta Biomater 2010; 6(12):4476-87; PMID:20624495; http://dx.doi.org/10.1016/j.actbio.2010.07.006
15. Sun JS, Liu HC, Chang WH, Li J, Lin FH, Tai HC. Influence of hydroxyapatite particle size on bone cell activities: an in vitro study. J Biomed Mater Res 1998; 39:390-7; PMID:9468047; http://dx.doi.org/10.1002/(SICI)1097-4636(19980305)39:3%3c390::AID-JBM7%3e3.0.CO;2-E
16. Shi Z, Huang X, Cai Y, Tang R, Yang D. Size effect of hydroxyapatite nanoparticles on proliferation and apoptosis of osteoblast-like cells. Acta Biomater 2009; 5(1):338-45; PMID:18753024; http://dx.doi.org/10.1016/j.actbio.2008.07.023
17. Jung UW, Choi SY, Pang EK, Kim CS, Choi SH, Cho KS. The effect of varying the particle size of beta tricalcium phosphate carrier of recombinant human bone morphogenetic protein-4 on bone formation in rat calvarial defects. J Periodontol 2006; 77(5):765-72; PMID:16671867; http://dx.doi.org/10.1902/jop.2006.050268
18. Carvalho AL, Faria PE, Grisi MF, Souza SL, Taba MJ, Palioto DB, Novaes AB, Fraga AF, Ozyegin LS, Oktar FN, Salata LA. Effects of granule size on the osteoconductivity of bovine and synthetic hydroxyapatite: a histologic and histometric study in dogs. J Oral Implantol 2007; 33(5):267-76; PMID:17987858; http://dx.doi.org/10.1563/1548-1336(2007)33%5b267:EOGSOT%5d2.0.CO;2
19. Malard O, Bouler JM, Guicheux J, Heymann D, Pilet P, Coquard C, Daculsi GJ. Influence of biphasic calcium phosphate granulometry on bone ingrowth, ceramic resorption, and inflammatory reactions: preliminary in vitro and in vivo study. J Biomed Mater Res 1999; 46:103-11; PMID:10357141; http://dx.doi.org/10.1002/(SICI)1097-4636(199907)46:1%3c103::AID-JBM12%3e3.0.CO;2-Z
20. Cheung HS, Devine TR, Hubbard W. Calcium phosphate particle induction of metalloproteinase and mitogenesis: effect of particle sizes. Osteoarthritis Cartilage 1997; 5:145-51; PMID:9219677; http://dx.doi.org/10.1016/S1063-4584(97)80009-X
21. Gauthier O, Bouler JM, Weiss P, Bosco J, Aguado E, Daculsi G. Short-term effects of mineral particle sizes on cellular degradation activity after implantation of injectable calcium phosphate biomaterials and the consequences for bone substitution. Bone 1999; 25(2 Suppl):71S-4S.; http://dx.doi.org/10.1016/S8756-3282(99)00137-4
22. Pallesen L, Schou S, Aaboe M, Hjørting-Hansen E, Nattestad A, Melsen F. Influence of particle size of autogenous bone grafts on the early stages of bone regeneration: a histologic and stereologic study in rabbit calvarium. Int J Oral Maxillofac Implants 2002 Jul-Aug; 17(4):498-506; PMID:12182292
23. Weissenboeck M, Stein E, Undt G, Ewers R, Lauer G, Turhani D. Particle size of hydroxyapatite granules calcified from red algae affects the osteogenic potential of human mesenchymal stem cells in vitro. Cells Tissues Organs 2006; 182(2):79-88; http://dx.doi.org/10.1159/000093062
24. Oonishi H, Hench LL, Wilson J, Sugihara F, Tsuji E, Kushitani S, Iwaki H. Comparative bone growth behavior in granules of bioceramic materials of various sizes. J Biomed Mater Res 1999; 44(1):31-43; PMID:10397902; http://dx.doi.org/10.1002/(SICI)1097-4636(199901)44:1%3c31::AID-JBM4%3e3.0.CO;2-9
25. Evans EJ. Toxicity of hydroxyapatite in vitro: the effect of particle size. Biomaterials 1991; 12(6):574-6; PMID:1663393; http://dx.doi.org/10.1016/0142-9612(91)90054-E
26. Lange T, Schilling AF, Peters F, Mujas J, Wicklein D, Amling M. Size dependent induction of proinflammatory cytokines and cytotoxicity of particulate beta- tricalciumphosphate in vitro. Biomaterials 2011; 32(17):4067-75; PMID:21421269; http://dx.doi.org/10.1016/j.biomaterials.2011.02.039
27. AlGhamdi AS, Shibly O, Ciancio SG. Osseous grafting part I: autografts and allografts for periodontal regeneration–a literature review. J Int Acad Periodontol 2010; 12(2):34-8
28. Zaner DJ, Yukna RA. Particle size of periodontal bone grafting materials. J Periodontol 1984; 55(7):406-9; PMID:6086869; http://dx.doi.org/10.1902/jop.1984.55.7.406
29. Coathup MJ, Cai Q, Campion C, Buckland T, Blunn GW. The effect of particle size on the osteointegration of injectable silicate-substituted calcium phosphate bone substitute materials. J Biomed Mater Res B Appl Biomater 2013; 101(6):902-10; PMID:23362131; http://dx.doi.org/10.1002/jbm.b.32895
30. Bohner M, Baumgart F. Theoretical model to determine the effects of geometrical factors on the resorption of calcium phosphate bone substitutes. Biomaterials 2004; 25(17):3569-82; PMID:15020131; http://dx.doi.org/10.1016/j.biomaterials.2003.10.032
31. Dietze S, Bayerlein T, Proff P, Hoffmann A, Gedrange T. The ultrastructure and processing properties of Straumann Bone Ceramic and NanoBone. Folia Morphol (Warsz) 2006; 65(1):63-5; PMID:16783740
32. Ghanaati SM, Thimm BW, Unger RE, Orth C, Kohler T, Barbeck M, Müller R, Kirkpatrick CJ. Collagen-embedded hydroxylapatite-beta-tricalcium phosphate-silicon dioxide bone substitute granules assist rapid vascularization and promote cell growth. Biomed Mater 2010; 5(2):25004; PMID:20208127; http://dx.doi.org/10.1088/1748-6041/5/2/025004
33. Ghanaati S, Orth C, Barbeck M, Willershausen I, Thimm BW, Booms P, Stübinger S, Landes C, Sader RA, Kirkpatrick CJ. Histological and histomorphometrical analysis of a silica matrix embedded nanocrystalline hydroxyapatite bone substitute using the subcutaneous implantation model in Wistar rats. Biomed Mater 2010; 5(3):035005; PMID:20460687
34. Ghanaati S, Barbeck M, Hilbig U, Hoffmann C, Unger RE, Sader RA, Peters F, Kirkpatrick CJ. An injectable bone substitute composed of beta-tricalcium phosphate granules, methylcellulose and hyaluronic acid inhibits connective tissue influx into its implantation bed in vivo. Acta Biomater 2011; 7(11):4018-28;

PMID:21784183; http://dx.doi.org/10.1016/j.actbio.2011.07.003
35. Barbeck M, Udeabor S, Lorenz J, Schlee M, Grosse Holthaus M, Raetscho N, Choukroun J, Sader R, Kirkpatrick CJ, Ghanaati S. High-temperature sintering of xenogeneic bone substitutes leads to increased multinucleated giant cell formation: in vivo and preliminary clinical results. J Oral Implantol 2014; PMID:25105868
36. Barbeck M, Lorenz J, Grosse Holthaus M, Raetscho N, Kubesch A, Booms P, Sader R, Kirkpatrick CJ, Ghanaati S. Porcine dermis and pericardium-based, non cross-linked materials induce multinucleated giant cells after their in vivo implantation: a physiological reaction? J Oral Implantol 2014; PMID:25386662
37. Barbeck M, Udeabor SE, Lorenz J, Kubesch A, Choukroun J, Sader RA, Kirkpatrick CJ, Ghanaati S. Induction of multinucleated giant cells in response to small sized bovine bone substitute (Bio-Oss^{TM}) results in an enhanced early implantation bed vascularization. Ann Maxillofac Surg 2014 Jul-Dec; 4(2):150-7; PMID:25593863; http://dx.doi.org/10.4103/2231-0746.147106
38. Kokkinopoulou M, Güler MA, Lieb B, Barbeck M, Ghanaati S, Markl J. 3D-ultrastructure, functions and stress responses of gastropod (Biomphalaria glabrata) rhogocytes. PLoS One 2014; 9(6):e101078; PMID:24971744; http://dx.doi.org/10.1371/journal.pone.0101078
39. Hanaichi T, Sato T, Iwamoto T, Malavasi-Yamashiro J, Hoshino M, Mizuno N. A stable lead by modification of Sato's method. J Electron Microsc 1986; 35:304-6; PMID:2440973
40. Nasr HF, Aichelmann-Reidy ME, Yukna RA. Bone and bone substitutes. Periodontol 2000 1999; 19:74-86
41. Klawitter JJ, Hulbert SF. Application of porous ceramics for the attachment of load bearing internal orthopedic applications. J Biomed Mater Res Sympos 1971; 2:161; http://dx.doi.org/10.1002/jbm.820050613
42. Baldini M, DeSanctis M, Ferrari M. Deproteinized bovine bone in periodontal and implant surgery Dent Mater 2011; 27:61-70; PMID:21112618; http://dx.doi.org/10.1016/j.dental.2010.10.017
43. Schlegel AK, Donath K. BIO-OSS–a resorbable bone substitute? J Long Term Eff Med Implants 1998; 8(3–4):201-9; PMID:10186966
44. Cannon GJ, Swanson JA. The macrophage capacity for phagocytosis. J Cell Sci 1992; 101(Pt 4):907-13; PMID:1527185
45. Champion JA, Walker A, Mitragotri S. Role of particle size in phagocytosis of polymeric microspheres. Pharm Res 2008; 25(8):1815-21; PMID:18373181; http://dx.doi.org/10.1007/s11095-008-9562-y
46. Tabata Y, Ikada Y. Effect of the size and surface-charge of polymer microspheres on their phagocytosis by macrophage. Biomaterials. 1988; 9:356-362; PMID:3214660; http://dx.doi.org/10.1016/0142-9612(88)90033-6
47. Anderson JM. Biological responses to materials. Annu Rev Mater Res 2001; 31:81-110; http://dx.doi.org/10.1146/annurev.matsci.31.1.81
48. Jayaraman M, Meyer U, Bühner M, Joos U, Wiesmann HP. Influence of titanium surfaces on attachment of osteoblast-like cells in vitro. Biomaterials 2004; 25 (4):625-31; PMID:14607500; http://dx.doi.org/10.1016/S0142-9612(03)00571-4
49. Marchisio M, Di Carmine M, Pagone R, Piattelli A, Miscia S. Implant surface roughness influences osteoclast proliferation and differentiation. J Biomed Mater Res B Appl Biomater 2005; 75(2):251-6; PMID:16078239; http://dx.doi.org/10.1002/jbm.b.30287
50. Miyanishi K, Trindade MC, Ma T, Goodman SB, Schurman DJ, Smith RL. Periprosthetic osteolysis: induction of vascular endothelial growth factor from human monocyte/macrophages by orthopaedic biomaterial particles. J Bone Miner Res 2003; 18(9):1573-83; PMID:12968666; http://dx.doi.org/10.1359/jbmr.2003.18.9.1573
51. Brown BN, Ratner BD, Goodman SB, Amar S, Badylak SF. Macrophage polarization: an opportunity for improved outcomes in biomaterials and regenerative medicine. Biomaterials 2012; 33(15):3792-802; PMID:22386919; http://dx.doi.org/10.1016/j.biomaterials.2012.02.034
52. Yang YQ, Tan YY, Wong R, Wenden A, Zhang LK, Rabie AB. The role of vascular endothelial growth factor in ossification. Int J Oral Sci 2012; 4(2):64-8; PMID:22722639; http://dx.doi.org/10.1038/ijos.2012.33
53. McNally AK, Anderson JM. Multinucleated giant cell formation exhibits features of phagocytosis with participation of the endoplasmic reticulum. Exp Mol Pathol 2005; 79(2):126-35; PMID:16109404; http://dx.doi.org/10.1016/j.yexmp.2005.06.008
54. Flannagan RS, Jaumouillé V, Grinstein S. The cell biology of phagocytosis. Annu Rev Pathol 2012; 7:61-98; PMID:21910624; http://dx.doi.org/10.1146/annurev-pathol-011811-132445
55. Brodbeck WG, Anderson JM. Giant cell formation and function. Curr Opin Hematol 2009; 16(1):53-7; PMID:19057205; http://dx.doi.org/10.1097/MOH.0b013e32831ac52e
56. Roodman GD. Cell biology of the osteoclast. Exp Hematol 1999; 27(8):1229-41; PMID:10428500; http://dx.doi.org/10.1016/S0301-472X(99)00061-2
57. Blair HC. How the osteoclast degrades bone. Bioessays 1998; 20(10):837-46; PMID:9819571; http://dx.doi.org/10.1002/(SICI)1521-1878(199810)20:10%3c837::AID-BIES9%3e3.0.CO;2-D
58. Stenbeck G. Formation and function of the ruffled border in osteoclasts. Semin Cell Dev Biol 2002; 13 (4):285-92; PMID:12243728; http://dx.doi.org/10.1016/S1084952102000587
59. Väänänen HK, Horton M. The osteoclast clear zone is a specialized cell-extracellular matrix adhesion structure. J Cell Sci 1995; 108(Pt 8):2729-32
60. Coxon FP, Taylor A. Vesicular trafficking in osteoclasts. Semin Cell Dev Biol 2008; 19(5):424-33; PMID:18768162; http://dx.doi.org/10.1016/j.semcdb.2008.08.004
61. Halleen JM, Alatalo SL, Suominen H, Cheng S, Janckila AJ, Väänänen HK. Tartrate-resistant acid phosphatase 5b: a novel serum marker of bone resorption. J Bone Miner Res 2000; 15(7):1337-45; PMID:10893682; http://dx.doi.org/10.1359/jbmr.2000.15.7.1337